A discrete and stochastic simulation model for migration of fish with application to capelin in the seas around Iceland

Kjartan G. Magnússon, Sven Th. Sigurdsson and Baldvin Einarsson

Science Institute, University of Iceland, Dunhaga 3, 107 Reykjavík, Iceland

Abstract. An individual based, discrete and stochastic model for the collective motion of fish presented in Hubbard *et al*. (2004) is applied to the task of simulating migrations of capelin in the seas around Iceland. In this application the individual particles may be viewed as small schools of fish that are self-propelled and interacting in such a way that the motion is governed on one hand by a tendency to imitate the motion of other particles in a local neighbourhood and on the other hand by external environmental vector fields for temperature, food density and oceanic currents, as well as a force field generated by an attracting spawning region. In addition there is a stochastic component. The implementation of this model is based on a triangularization of the region under consideration which is shown to be advantageous both in terms of computational efficiency and access to external data. Results of simulations are presented showing the migration pattern of capelin that is situated north-west off Iceland at the beginning October and migrates to spawning grounds south off Iceland by the end of March the following year.

Key words: Fish migration; Interacting particle model; Stochastic model; Capelin; Environmental fields.

Introduction

Many species of fish undertake extensive movements between feeding and spawning grounds. Such directed movements between specific areas – as opposed to random dispersal – are referred to as migrations. Fish migrations are as yet a poorly understood phenomenon; the general route the fish take – which may be genetically "programmed" in some way – are usually fairly well known as well as the approximate timing, but there is considerable year to year variation, presumably due to varying oceanographical conditions. The migration is also influenced by the physiological condition of the fish which is governed by the food density and distribution. How the spatio-temporal characteristics of migrations are affected by the environment is not well known, apart from some general observations. Oceanographic variables which clearly have an effect on migrations are temperature, oceanic currents and food density amongst others.

The capelin (*Mallotus villosus*) in the central North–Atlantic is a good example of a migrating stock illustrating the above. The migrations of the Icelandic capelin are discussed in detail in Vilhjálmsson (1994) and the main features summarized in Hubbard *et al* (2004). We will therefore only give a very brief account here. The spawning stock appears in the waters off the north-east coast of Iceland in late autum-early winter from feeding grounds in the north around the island of Jan Mayen. The stock moves slowly clockwise around Iceland and ends up on the spawning grounds

on the south and south-west coast in March-April. A component of the stock takes a more direct route, counter-clockwise around the island. The size of this component is very variable and is possibly connected to the temperature distribution in the ocean. In this paper we will attempt to model the effects of oceanographical conditions on the spawning migrations of capelin in Icelandic waters.

The collective movements of groups of animals can be modelled as a continuous system in time and density (Okubo and Levin, 2001; Toner and Tu, 1998; Babak *et al*., 2004), or as individual based system, which may be discrete (e.g. Vicsek *et al*., 1995) or continuous (Niwa, 1998) in time. The migrations of capelin around Iceland and in the Barents Sea have been modelled by a continuous density Kolmogorov type model (Magnússon *et al*, 2004; Magnússon *et al*., in press) and by a discrete individual based stochastic model (Hubbard *et al*, 2004), where individual fish or schools are regarded as self-propelled interacting particles. Both these models are generic in the sense that they can be applied to any stock and area.

The model presented here extends the one presented in Hubbard *et al*. (2004) firstly in that it includes a field of currents that may carry the fish along. Since typical sea current speeds can be of the same order of magnitude as the speed of fish relative to the surrounding sea this may have a significant effect on the migration pattern. Secondly we present a more general approach to deal with attraction to spawning grounds. This allows us, in particular, to include complex obstacles (e.g. islands) in the path of the fish, without the problem of fish getting "stuck" by being pulled into these obstacles by the attraction. This new approach further allows us to include the effect of attraction to spawning grounds in the same comfort function that includes the effects of sea temperature and food density on the motion of the fish. Our approach here is identical to the one adopted in Dereksdóttir *et al*. (2003), in the context of a continuous Kolmogorov-type model of fish migration. In the context of the particle model presented here, the result of this new approach is that we now first group the effects of sea temperature on the direction of motion together with the effects of spawning attraction, rather than first grouping them with the effects of alignment as is done in Hubbard *et al*. (2004).

We also present here a new implementation of the model by introducing a triangularization, that may be fully unstructured, of the region under consideration and subsequently applying the model locally within these triangular elements. Our main reasons for adopting such an implementation are:

1. It allows us to deal effectively with data described in terms of longitude and latitude. Much of the available data on oceanographical conditions as well as fishery is described in this way.
2. It allows us to introduce good approximations to obstacles of complex shape by describing them as a union of unstructured triangular elements.
3. It provides us with a framework of keeping track of neighbour particles, within the same element or within neighbour elements, which in turn makes the calculation of alignment computationally more efficient.
4. It allows us to share data files and make effective comparisons with continuous migration models that we have also developed, since a finite element implementation of those models is based on exactly the same triangular subdivision.

We finally demonstrate the feasibility of this approach by presenting the results of numerical simulations of capelin migration around Iceland towards its spawning grounds from October 1 till April 1 the following spring for 1994-1995, which was a cold year, and 2000-2001, which was a warm year, using the same data as in Dereksdóttir *et al*. (2003).

Mathematical model

The model consists of a collection of particles (fish or small fish schools) moving in a plane, within a prescribed domain. The particles are self-propelling, but are also being carried by a time dependent vector field of currents, $\boldsymbol{V}_c(\boldsymbol{x};t)$, specified external to the model. Particle *i* has speed $v_i(t)$ relative to the field of currents, and a direction of motion given by the angle θ_i. The general dynamical equation for the position of the *i*-th particle is

$$\boldsymbol{x}_i(t+\Delta t) = \boldsymbol{x}_i(t) + \left(\boldsymbol{V}_i(t) + \boldsymbol{V}_c(\boldsymbol{x}_i(t);t)\right)\Delta t \tag{1}$$

where

$$\boldsymbol{V}_i(t) = \frac{v_i(t)}{\left\|\left(1-\beta_i(t)\right)\boldsymbol{p}_i(t) + \beta_i(t)\boldsymbol{q}_i(t)\right\|}\left(\left(1-\beta_i(t)\right)\boldsymbol{p}_i(t) + \beta_i(t)\boldsymbol{q}_i(t)\right) \tag{2}$$

and the unit vector $\boldsymbol{p}_i(t)$ represents the effect of neighbouring particles on the direction of motion, whereas the unit vector $\boldsymbol{q}_i(t)$ is determined by the gradient of a function $U(\boldsymbol{x};t)$, which we refer to as a comfort function (Reed and Balchen, 1982). This function will incorporate the factors, which are believed to affect the "comfort" or well-being of the fish, such as temperature, food density, location relative to the spawning grounds, etc.

$\theta_{\boldsymbol{p},i}(t)$, the direction angle of $\boldsymbol{p}_i(t)$ is calculated similarly as in Vicsek et al. (1995) i.e. by

$$\theta_{\boldsymbol{p},i}(t) = \left\langle \theta_j(t-\Delta t)\right\rangle_{i,\rho} + \xi_i^t \tag{3}$$

where $\left\langle \theta_j \right\rangle_{i,\rho}$ denotes the average angle of motion of all particles inside a circle of radius ρ centered on the *i*-th particle. The average angle is calculated by taking the direction angle of the average of individual direction vectors of these particles at the previous time $t-\Delta t$. The term ξ_i^t is a random perturbation of the direction angle which we choose either as a uniform noise within the interval $[-\eta/2, \eta/2]$ and add in fact to the angle of $\left(1-\beta_i(t)\right)\boldsymbol{p}_i(t) + \beta_i(t)\boldsymbol{q}_i(t)$ rather than $\boldsymbol{p}_i(t)$, or as a "directional noise" described in more detail below.

The comfort function used here is the same as presented in Magnússon *et al*. (2004). It is a linear combination of functions of temperature and food density and a potential function

$$U(\mathbf{x};t) = \alpha_1(t)r\left(T(\mathbf{x};t)\right) + \alpha_2(t)s\left(f(\mathbf{x};t)\right) + \alpha_3(t)\phi(\mathbf{x}) \tag{4}$$

where $T(\mathbf{x};t)$ and $f(\mathbf{x};t)$ are the temperature and food density respectively at location $\mathbf{x}$ at time t and r and s are given functions defined as follows:

$$r(T) = \begin{cases} -(T - T_1)^4 & \text{if} \quad T \le T_1 \\ 0 & \text{if} \quad T_1 \le T \le T_2 \\ -(T - T_2)^2 & \text{if} \quad T_2 \le T \end{cases} \tag{5}$$

and

$$s(f) = \frac{f}{h + f} \tag{6}$$

where T_1, T_2 and h are constants. The functional form of r implies that the preferred temperature range is between T_1 and T_2 degrees. The fish tend to move towards areas where the temperature is within the preferred range and this tendency is stronger in cold waters. The preferred temperature range may vary within the year. The function s is an asymptotic and increasing function of food density, f. This functional form implies that the tendency to move towards areas of higher food density decreases with increasing density and is virtually nil at high food densities. The α-coefficients in (4) will be specified later.

The function ϕ is a potential function for the attraction towards the spawning grounds and is defined as follows:

Let the region in which the fish can move be denoted by Ω. We define the boundary of Ω to be any lines, which the fish are not able to cross, such as the coastlines and possibly certain isotherms. The region is in general not simply connected since it may have one or more "holes" in it. Assume that the spawning grounds cover a sub-area S of Ω and that migrating fish are attracted towards S, in the sense that they experience a "force field" pulling them towards it. The spawning region may be regarded as a continuous sink spread over S, to use an analogy from fluid dynamics, and we define the sink density (analogous to mass density or charge density) in the spawning region S by $\rho(\mathbf{x})$. The total attraction strength (sink strength) of the spawning area is therefore given by

$$m = \iint_S \rho dA \tag{7}$$

The potential ϕ is given as the solution of Poisson's equation

$$\Delta\phi = -\rho \qquad \text{in } \Omega \tag{8}$$

subject to no-flux condition at the obstacle boundaries of Ω, i.e.

$$\frac{\partial\phi}{\partial n} = 0 \qquad \text{on } \partial\Omega \tag{9}$$

The force field attracting the fish towards the spawning grounds is given by the gradient of ϕ, $\nabla\phi$. The gradient is orthogonal to the equipotential lines and is therefore tangent to the set of lines known as streamlines, which the fish would travel along if there were no other factors influencing the motion, than possible obstacles in the form of holes within Ω, that the fish cannot cross.

In the case of an infinite region Ω with no boundaries or obstacles and an attracting region consisting of a single point of sink strength *m,* located at the origin, the attraction density is $\rho(\boldsymbol{x}) = m\delta(\boldsymbol{x})$, where $\delta(\boldsymbol{x})$ is the delta function. The corresponding potential function is

$$\phi(\boldsymbol{x}) = -\frac{m}{2\pi}\ln\|\boldsymbol{x}\| \tag{10}$$

and the streamlines are simply straight lines through the origin. In the case of a finite region we have to specify boundary conditions at the outer boundaries of the region. Rather than viewing them as non-obstacle boundaries we specify the ϕ-values on the outer boundary according to (10), approximating the spawning region S by a single point.

One way of quantifying the weight β in equation (2) is to let it depend on the time constants associated with how quickly the particle adjusts its direction to that governed by alignment on one hand and the gradient of the comfort function on the other. Assuming that the former time constant is Δt and the latter is $\sigma\Delta t$ we have that

$$\beta = \frac{1/(\sigma\Delta t)}{1/\Delta t + 1/(\sigma\Delta t)} = \frac{1}{1+\sigma} \tag{11}$$

Also note in this context that equations (1) and (2) may be viewed as an explicit time discretization of the following dynamical system:

$$\frac{d}{dt}\begin{bmatrix}\boldsymbol{x}_i(t)\\ \hat{\boldsymbol{V}}_i(t)\end{bmatrix} = \begin{bmatrix}\hat{\boldsymbol{V}}_i(t) + \boldsymbol{V}_c(\boldsymbol{x}_i, t)\\ \frac{1}{\tau}\left(\boldsymbol{V}_i(t) - \hat{\boldsymbol{V}}_i(t)\right)\end{bmatrix} \tag{12}$$

with $\boldsymbol{V}_i(t)$ being defined according to equation (2) and the time constant of how quickly the velocity $\boldsymbol{V}_i(t)$ adjusts to the set velocity $\boldsymbol{V}_i(t)$ being $\tau = \Delta t$.

Returning to the question of noise, an alternative to the formulation presented above, with uniform noise around the angle of the vector $(1-\beta_i(t))\,\boldsymbol{p}_i(t) + \beta_i(t)\boldsymbol{q}_i(t)$,

is to adopt the approach given in Hubbard *et al*. (2004) and introduce a "directional noise", $\hat{\xi}_i^t$, around $\theta_{\boldsymbol{p},i}(t)$, the angle of the vector $\boldsymbol{p}_i(t)$, in the direction of $\theta_{\boldsymbol{q},i}(t)$, the angle of the vector $\boldsymbol{q}_i(t)$. We can for example define the probability density function of $\hat{\xi}$ as a linear function on a finite interval around 0

$$p_{\hat{\xi}}(x) = \frac{2\gamma}{\eta^2}x + \frac{1}{\eta} \qquad -\frac{\eta}{2} \le x \le \frac{\eta}{2} \tag{13}$$

where

$$\gamma = \kappa_\theta \frac{\theta_{\boldsymbol{q},i}(t) - \theta_{\boldsymbol{p},i}(t)}{\pi} \qquad 0 \le \kappa_\theta \le 1 \tag{14}$$

(see Fig. 1). In general, κ_θ will be taken to be either zero or one, i.e. the directional noise is switched on or switched off. Note that $-\pi < \theta_{\boldsymbol{q},i}(t) - \theta_{\boldsymbol{p},i}(t) \le \pi$ and thus $|\gamma| \le \kappa_\theta \le 1$ ensuring that $p_{\hat{\xi}}(x) \ge 0$. The expected value of $\hat{\xi}$ is

$$E\left[\hat{\xi}\right] = \frac{\gamma\eta}{6} \tag{15}$$

and hence

$$E\left[\theta_{\boldsymbol{p},i}(t) + \hat{\xi}_i^t\right] = (1-\beta)\theta_{\boldsymbol{p},i}(t) + \beta\theta_{\boldsymbol{q},i}(t) \quad \text{with} \quad \beta = \frac{\kappa_\theta\eta}{6\pi} \tag{16}$$

Thus if $\kappa_\theta = 1$, $\eta = 2\pi$ and the time constant associated with alignment is Δt then the expected time constant associated with adjustment to the direction of the gradient of the comfort function will be $\sigma\Delta t$ where $\sigma = \frac{1}{\beta} - 1 = 2$ (cf. (11)) and this time constant increases as η decreases.

The variance is

$$V\left[\hat{\xi}\right] = \frac{\eta^2}{36}\left(3 - \gamma^2\right) \tag{17}$$

Thus the variance with the directional nose "off", i.e. $\kappa_\theta = 0$, is $\frac{\eta^2}{12}$, but decreases as the directional noise is "switched on", i.e. $\frac{\eta^2}{18} \le V\left[\hat{\xi}_{\kappa_\theta=1}\right] \le \frac{\eta^2}{12}$, depending on $\theta_{\boldsymbol{q},i}(t) - \theta_{\boldsymbol{p},i}(t)$.

We can also introduce in a similar manner a noise component, ζ_i^t, to the speed with probability density given by

$$p_\zeta(x) = \frac{2\lambda}{\mu^2}x + \frac{1}{\mu} \qquad -\frac{\mu}{2} \le x \le \frac{\mu}{2} \tag{18}$$

where

$$\lambda = \kappa_v \max\left\{\min\left\{v_0 - v_i(t), 1\right\}, -1\right\} \quad 0 \le \kappa_v \le 1 \tag{19}$$

Here v_0 is a reference speed or an average cruising speed. Thus particles which are moving slower than the reference speed are more likely to speed up than slow down and particles moving faster are more likely to slow down. The above formulation of λ ensures that $|\lambda| \le \kappa_v \le 1$ and hence that $p_\zeta(x) \ge 0$.

Finally, we note that in addition to the directions $\boldsymbol{p}_i(t)$, representing the effect of neighbouring particles on the direction of motion, and $\boldsymbol{q}_i(t)$, the direction of the gradient of the comfort function $U(\boldsymbol{x};t)$, that determine the direction of velocity according to equation (2), it may be of interest to include a third direction $\boldsymbol{r}_i(t)$ the role of which is to try to maintain some prescribed preferred density of particles. Thus if the density is below this preferred value this direction should be towards an area where the density is greater, e.g. in the direction of the gradient of the density, if it can be represented as a continuous differentiable function. If the density is above the prescribed value the direction should be towards an area where the density is smaller. The relative weight of such a direction could depend on how much the actual density deviates from the preferred one. We have already noted that the interplay between a stochastic component and the effect of alignment may play a role in the formation of schools. The inclusion of a density effect may also play a significant role in school formation as indicated by the analysis presented in Babak *et al*. (2004) in the case of a continuous dynamic model.

Numerical implementation

In our numerical implementation of the mathematical model we introduce a triangularization of the region under consideration, that may be fully unstructured. Obstacles (islands) within the region are simply specified by identifying some of the triangular elements as "land" elements. For each triangular element ΔABC we introduce a local (*x*,*y*)-coordinate system as shown in Fig. 2 where the local coordinates of the corner points

$$A = \langle 0,0 \rangle \quad B = \langle a,0 \rangle \quad C = \langle b,c \rangle \tag{20}$$

are readily evaluated from the distances between the corner points:

$$a = |AB|, \quad b = \frac{a^2 + |AC|^2 - |BC|^2}{2a}, \quad c = \sqrt{|AC|^2 - b^2} \tag{21}$$

When these corner points are specified globally in terms of longitude, Θ, and latitude, Φ, as is usually the case in our applications, these distances are in turn readily calculated from the corresponding cartesian coordinates:

$$X = R\cos\left(\frac{\Phi\pi}{180}\right)\cos\left(\frac{\Theta\pi}{180}\right), \quad Y = R\cos\left(\frac{\Phi\pi}{180}\right)\sin\left(\frac{\Theta\pi}{180}\right), \quad Z = R\sin\left(\frac{\Phi\pi}{180}\right) \quad (22)$$

R = 6350km being the radius of the earth. We may calculate these distances either as direct cartesian distances or as great circle distances, the approximation in either case being that we are approximating the triangular element on the sphere with a flat element. This approximation has a negligible effect in our application. We avoid on the other hand having to introduce any global projection on to a plane which may result in more serious distortions. In addition to these local coordinates we calculate the angle from the global west-east direction to the edge AB as:

$$u = \tan^{-1}\left(\frac{\Phi_B - \Phi_A}{\cos\Phi_A\left(\Theta_B - \Theta_A\right)}\right) \quad (23)$$

where the value of the angle is changed by π when $\Theta_A > \Theta_B$.

For each particle, number *i*, under consideration we keep the following information:

i the identification number of the particle.
E ($\hat{E}$) the number of the element that the particle is within now (after motion).
x, y ($\hat{x}, \hat{y}$) the local coordinates of the particle within that element now (after motion).
θ ($\hat{\theta}$) the local angle of the previous (next) direction of motion of the particle.
v the present speed of the particle.

For each nodal point, number *j*, in the net of elements we keep the following information:

j the identification number of the nodal point.
Θ, *Φ* the global coordinates of the point (longitude and latitude).
U the present value of the comfort function at the point.

For each triangular element, number *k*, in the net we keep the following information:

k the identification number of the element (-1 if the element is a "land" element).
N_A, N_B, N_C the identification numbers of its three corner points
a,*b*,*c* the local coordinate values of its corner points
u the angle that the *AB*-edge makes with the global west-east direction
E_A, E_B, E_C the identification numbers of its three neighbour elements, adjacent to the element edges opposite the points A,B,C (0 if there is no neighbour element).
$\mathbf{V}_c$ the present velocity current vector within the element

In addition, for the sake of computational efficiency, we may maintain a list of the numbers of those elements that presently contain any particles, as well as maintaining for such elements a list of the numbers of those particles that are presently within the element. On the basis of this information the positions of the particles can now be updated in turn as follows:

We calculate the angle of the alignment unit vector $\boldsymbol{p}_i(t)$ locally within the element, by letting the alignment only depend on those particles that are within a specified distance, ρ, as well as being within the same element or one of its three neighbour elements, cf. Fig. 3. The second additional restriction is included for the sake of computational efficiency. In order to check whether a particle at point P', within a neighbour element, should affect the alignment of the particle at point P, we firstly check whether $|PQ| > \rho$, where Q is the projection of P onto the common edge. If that is so we subsequently check whether $\left(|PQ| + |P'Q'|\right)^2 + |QQ'|^2 > \rho^2$ where Q' is the projection of P' onto the common edge. The lengths of these line segments can all be easily calculated locally. If such a particle in a neighbour element is to be included the corresponding local angle θ' can be changed into the local coordinates of the original element by the transformation

$$\theta = \theta' + u' - u \tag{24}$$

cf. Fig. 4. The direction angle of $\boldsymbol{p}_i(t)$ can subsequently be calculated as:

$$\tan^{-1}\left(\frac{\sum_j \sin\theta_j}{\sum_j \cos\theta_j}\right) \tag{25}$$

where we sum over all particles satisfying the distance conditions, and the value of the angle is changed by π when the denominator of the argument is negative.

We calculate the angle of the comfort gradient unit vector $\boldsymbol{q}_i(t)$ locally within the element, from the specified comfort values $U_A(t), U_B(t), U_C(t)$, at its three corner points, assuming that the comfort function is linear within the element. Then we have that within the element

$$\nabla U(t) = \frac{-1}{ac}\begin{bmatrix} c & -c & 0 \\ a-b & b & -a \end{bmatrix}\begin{bmatrix} U_A(t) \\ U_B(t) \\ U_C(t) \end{bmatrix} \quad \text{and} \quad \boldsymbol{q}(t) = \frac{1}{\|\nabla U(t)\|}\nabla U(t) \tag{26}$$

noting that the columns of the matrix are in fact outward normal vectors on the edges opposite A, B, C respectively whose lengths are that of the corresponding edge.

Since the particle speed, $v(t)$, is specified with the particle and the current velocity $\boldsymbol{V}_c(t)$ with the element we can now calculate the new position of the particle according to equation (1) as well as the corresponding angle of the direction of motion in the local coordinates, and subsequently establish whether the new position falls within the

same element or not. If it does we simply update these values. If it does not, we first have to calculate the point of intersection, *I*, with the outgoing edge (see Fig. 4), the distance that the particle has travelled when hitting the edge ($|PI|$ in Fig. 4), and the distance of the point of intersection from the preceeding corner point in an anticlockwise direction ($|BI|$ in Fig. 4). From this we can readily establish the local coordinates of this point within the neighbour element, as well as the local angle of direction, θ', from equation (24), and hence continue the motion for the remaining distance $|IP'|$. This may lead us to a new edge in which case the above procedure is repeated. It is also possible that there is no neighbour element or that it turns out to be a land element. In that case the particle is reflected back into the same element for the remaining distance, the local angle of motion changing from θ to $\theta + 2(w - \theta) = 2w - \theta$, where *w* is the angle between the outgoing edge and the edge *AB* of the element (see Fig. 5). If the particle changes elements we update the new element number as well as the coordinates and angle with respect to that element. Note that, while dealing with the particles in turn, we have to keep separate records of positions and angles before and after motion since the alignment depends on the motion of the neighbour elements during the previous time step.

Note that with this implementation we are applying a reflective boundary condition, according to the terminology introduced in Hubbard *et al*. (2004), both at outer boundaries as well as obstacle boundaries. We may effectively replace these conditions by repulsion boundary conditions, according to the same terminology, by introducing at such boundary points temperature values that are well outside the interval $[T_1, T_2]$ in equation (5) (eg. 1000°C), thus forcing $\boldsymbol{q}_i(t)$ to point away from the boundary.

Equations (8) and (9), determining the potential part of the comfort function (4), are solved by a Galerkin finite element method with piecewise linear functions on the same triangular net thus giving directly the values of this function at the nodal points. The temperature and food density parts of the comfort function are specified externally and have to be interpolated onto these nodal points. The same holds true for the sea current values except that they have to be interpolated onto the centroids of the elements.

When displaying the positions of the particles we need to know their global coordinates. These can approximately be calculated from the local coordinates as follows:

$$\Theta = \Theta_A + \frac{x\cos u - y\sin u}{R\cos\Phi_A} \qquad \Phi = \Phi_A + \frac{x\sin u + y\cos u}{R} \tag{27}$$

Finally, note that if we are interested in including the direction towards a preferred density, $\boldsymbol{r}_i(t)$, described at the end of the previous section it can e.g. be done as follows in the present setting: Let *d* denote the average density of particles within a triangular element, i.e. the number of particles within the element divided by the area of the element and let d_A, d_B, and d_C denote the average density of its three neighbour

elements, adjacent to the element edges opposite the points *A*, *B,* and *C* resp. Then we can set:

$$\nabla d(t) = \frac{1}{ac}\begin{bmatrix} c & -c & 0 \\ a-b & b & -a \end{bmatrix}\begin{bmatrix} d_A(t) \\ d_B(t) \\ d_C(t) \end{bmatrix} \quad \text{and} \quad \boldsymbol{r}(t) = \frac{1}{\|\nabla d(t)\|}\nabla d(t) \tag{28}$$

This approximation is based on the relationship

$$\frac{1}{|\Delta|}\iint_{\Delta} \nabla d \, dxdy = \frac{1}{|\Delta|}\oint_{\partial\Delta} d\,\boldsymbol{n} ds \tag{29}$$

where we are integrating over a triangular element, Δ, $|\Delta|$ denotes the area of this element, and we approximate the density value along an edge in the line integral with the average of the average density values over the two elements on each side of that edge. Thus we only need to keep track of the number of particles within each element.

Simulation example

We demonstrate the feasibility of this approach by presenting the results of numerical simulations of capelin migration around Iceland towards its spawning grounds from October 1 till April 1 the following spring for 1994-1995, which was a cold year, and 2000-2001, which was a warm year, using the same data as in Dereksdóttir *et al*. (2003).

The area being considered is an area around Iceland extending from longitude 10°W to 30.5°W and from latitude 62°N to 69°N shown in Fig. 6. The triangular elements are aligned in such a way that one side has a fixed longitude and one side a fixed latitude. Each element spans 0.25° in longitude and 0.125° in latitude. Thus we have in total 9184 elements and 4731 nodal points. The size of the triangular elements varies from 90.1 km^2 in the south to 68.8 km^2 furthest north. The land elements describing Iceland are shown in Fig. 6. Greenland also extends into the north-west corner of this area, but has not been marked since the temperature of the sea in fact prevents the capelin from entering that part of the area.

In the comfort function we ignore the effect of food density by setting $\alpha_2 = 0$ in equation (4). Thus the vector $\boldsymbol{q}_i(t)$ in equation (2) only depends on the ratio $\alpha_1(t)/\alpha_3(t)$. We set $\alpha_3 = 0$ for the first 80 days and thereafter

$$\alpha_1/\alpha_3 = \begin{cases} 1/24 & \text{if } 80 \le t < 130 \\ 1/1920 & \text{if } 130 \le t < 182 \end{cases} \tag{28}$$

The preferred temperature range $[T_1, T_2]$ in equation (5) varies from [0.5,4.0] degrees on October 1 to [3.0,7.5] on April 1, the end values increasing linearly in time throughout this period. This is based on various field observations as described more

fully in Magnússon *et al*. (in press). The temperature fields for the ocean around Iceland are the same as constructed in in Dereksdóttir *et al*. (2003).

The radius of alignment, ρ, is set equal to 10 km. Since typical lengths of sides in the triangular elements are 12-16 km this implies that the circle of alignment will always extend into neighbour elements as shown in Fig. 3, and that some particles within that circle will in general not be counted for.

The weight-factor $\beta_i(t)$ in equation (2) is set equal to 0.9 for all particles at all times. The noise in the direction is uniform around the angle $\left(1-\beta_i(t)\right)\boldsymbol{p}_i(t)+\beta_i(t)\boldsymbol{q}_i(t)$ with a total range of $\eta = 80°$ (i.e. we do not implement the "directional noise").

The speed $v_i(t)$ changes with time as follows: it is constant for the first 80 days, 5 km/day, then increasing rapidly to 25 km/day during the following 50 days, and remaining at that value after that according to the expression

$$v(t) = \min\left(5 + 20 \cdot \frac{(t-80)^3}{50^3}, 25\right) \tag{29}$$

The hypothesis underlying this assumed increase is that the speed is related to the stage of maturity (i.e. roe content), which is increasing while the capelin are migrating as described more fully in Dereksdóttir *et al*. (2003). There is no noise included with the speed.

In order to include the effect of carrying sea currents we use the same hypothetical current field that is constructed in Dereksdóttir *et al*. (2003), which is meant to reflect the effects of the real currents around Iceland based on the information currently available (see Fig. 7). Note that the coastal current circulates Iceland in a clockwise direction. The speed of the hypothetical current is in the interval [0.75, 15] km/day and only varies with approximate distance from the shore.

The time step Δt is set at 0.1 days which implies that at the maximum speed of 25 km/day it takes the particle approximately 5 time steps to traverse each element. The number of particles is 1096 and at the start of the simulation at October 1 they are distributed over an area north-west of Iceland, as shown in Fig. 6, similar to the one used in the simulations in Dereksdóttir *et al*. (2003). The spawning area is specified south of Iceland as shown in Fig. 8. That figure also shows the gradient directions of the corresponding potential field obtained by solving equations (8) and (9).

Some snapshots of the result of a typical simulation run for the cold year 1994-1995 are shown in Fig. 9. The qualitative agreement with the results presented in Dereksdóttir *et al*. (2003) is good until February 1 but after that there is a discrepancy, mainly due the fact that a number of particles seem to get stuck in a couple of elements south-east off Iceland. The inclusion of the effect of a prescribed preferred density on the direction on movement, as described above, should however alleviate this type of problem. Snapshots of the result of a typical simulation run for the warm year 1994-1995, when a significant fraction of the capelin migrate down the west coast, are shown in Fig. 9. In this case the qualitative agreement with the results

presented in Dereksdóttir *et al*. (2003) is again good except that the distribution is more easterly on April 1.

Table 1: The relative distribution (%) in each of the sub-areas at four selected times for two simulations scenarios, the cold year 1994-95 and the warm year 2000-01. Average values of 10 independent runs with the same initial distribution.

Sub-area	Initial distrib.	November 1		January 1		February 15		April 1	
		1994	2000	1995	2001	1995	2001	1995	2001
1	0	0	0	0	0	0	3.1	0	0.6
2	7.1	1.5	0	8.6	18.0	0.4	23.7	0	0.9
3	22.8	10.1	0.1	14.4	23.7	0	0	0	0
4	0	0	0	0	0	9.8	4.8	5.0	3.0
5	0	7.0	0	9.7	6.8	1.1	0	0.2	0
6	0	2.0	0	46.0	21.1	0.6	0.4	0.3	0
7	0	0	0	0.3	0.2	0	0	0	0
8	0	0	0	0	0	7.7	0.5	0.2	0
9	0	0	0	0	0	3.3	50.1	3.6	58.8
10	0	0	0	0	0	0	0	7.1	19.3
11	70.1	75.8	97.6	0.3	0.5	0	0	0	0
12	0	2.7	0.4	20.6	24.0	0	0	0	0
13	0	0	0	0	0	77.1	17.4	83.6	17.3

Table 2. The relative distribution (%) in each of the sub-areas at four selected times for two simulations scenarios, the cold year 1994-95 and the warm year 2000-01. Average values of 20 independent runs with the same initial distribution.

Sub-area	Initial distrib.	November 1		January 1		February 15		April 1	
		1994	2000	1995	2001	1995	2001	1995	2001
1	0	0	0	0	0	0	2.0	0	0.5
2	7.1	1.2	0	7.3	12.5	0.3	17.0	0	0.8
3	22.8	10.1	0.1	12.8	20.4	0	0	0	0
4	0	0	0	0	0	9	4.0	5.2	2.6
5	0	5.8	0	7.6	7.5	0.7	0	0.2	0
6	0	2.6	0	49.9	26.7	0.5	0.3	0.2	0
7	0	0	0	0.8	0.1	0	0	0	0
8	0	0	0	0	0	6	0.4	0.1	0
9	0	0	0	0	0	2.8	55.4	3.1	59.1
10	0	0	0	0	0	0	0	5.8	22.1
11	70.1	76.0	97.9	0.4	0.8	0	0	0	0
12	0	3.3	0.4	21.1	28.3	0	0	0	0
13	0	0	0	0	0	80.6	20.9	85.3	14.9
14	0	0	0	0	0	0	0	0	0
15	0	0.5	1.5	0	3.6	0	0	0	0
16	0	0.5	0.1	0	0	0	0	0	0

In order to make a more quantitative comparison we show in Table 1 the average distribution for 10 independent simulation runs over 16 subareas around Iceland They correspond to the standard division, shown in Figure 12, that is based on the oceanographical, hydrographical and biological characteristics of the region (see Vilhjálmsson *et al*., 1997). Table 2 shows the same results for 20 independent runs. Comparing these latter results with those given in Dereksdóttir *et al*. (2003) the main discrepancy for 1994-1995 is that a larger fraction extends north into compartment 11 on November 1 (76.0% instead of 52.7%) and nort-east into compartment 12 on January 1 (21.1% instead 6.8%). By February 15 the majority (80.6%) has gone into compartment 13 instead of the majority (81.5%) being in compartment 9 and remains there on April 1 instead of moving into compartment 10. This discrepancy is mainly due to the large number of particles getting stuck in a few elements south-east of Iceland, as already mentioned. For 2000-2001 the results are very similar on November 1 but on January 1 a larger fraction has reached both west into compartment 2 (12.5% instead of 0.0%) and east into compartment 12 (28.3% instead of 2.6%). On February 15 there is still a larger fraction in compartment 2 (17.0% instead of 13.5%) and also a larger fraction that has reached compartment 13 (20.9% instead of 2.9%) and on April 1 the majority (59.1%) is in compartment 9 rather than the majority (79.9%) being in the more westerly compartment 10. Table 3 showing

Table 3. The relative distribution (%) in each of the sub-areas at four selected times for the simulations scenario in 2000-01. In the first variation the range of noise is reduced from 80° to 20° and in the second variation the number of particles is reduced from 1096 to 283. Average values of 10 independent runs with the same initial distribution.

Sub-area	Initial distrib.	November 1 2000		January 1 2001		February 15 2001		April 1 2001	
		Noise 10°	#part. 283	Noise 10°	#part. 283	Noise 10°	#part. 283	Noise 10°	#part. 283
1	0	0	0	0	0	7.8	0	0	0.8
2	7.1	0	0	24.9	2.8	35.9	11.6	0	1.0
3	22.8	0.2	0.1	13.3	35.8	0	0	0	0
4	0	0	0	0	0	0.9	5.4	0.9	3.5
5	0	0	0	4	13.9	0	0	0	0
6	0	0	0	27.6	35.8	0	0.8	0	0
7	0	0	0	0.4	0	0	0	0	0
8	0	0	0	0	0	0	1	0	0
9	0	0	0	0	0	40.5	58.3	35.4	32.8
10	0	0	0	0	0	0.1	0	49.8	52.0
11	70.1	94.9	99.5	0.9	2.5	0	0	0	0
12	0	0.1	0	14.6	8.9	0	0	0	0
13	0	0	0	0	0	14.9	22.9	13.9	9.9

corresponding results for 2000-01 when the noise range has been reduced on one hand and the number of particles on the other, however, serves as a remainder of the fact that the results are quite sensitive to such changes. We note for example that with both these changes the majority of particles ends up in compartment 10 on April 1 (cf. also Figure 11). But we also note on that while the variation between individual runs is

Table 4. Coefficient of variation (the ratio of the standard deviation and the average value) of the relative distribution in each of the sub-areas at February 15 for six different simulation scenarios, estimated from the indicated number of runs

.

Year	1995	2001	1995	2001	2001	2001
#particles	1096	1096	1096	1096	1096	283
#runs	10	10	30	30	10	10
Noiserange	80°	80°	80°	80°	20°	80°
Subarea						
1	0	1.40	0	1.69	1.20	0
2	0.86	0.81	1.04	0.97	0.51	0.42
3	0	0	0	0	0	0
4	0.43	1.00	0.64	1.02	1.16	0.48
5	0.78	0.03	1.06	0.05	0	0
6	0.75	0.91	0.83	1.02	0	0.70
7	0	0	0	0	0	0
8	0.51	1.38	0.64	1.30	0	0.58
9	0.36	0.36	0.45	0.28	0.42	0.07

considerable as can be deduced from the coefficient of variation values for February 15 presented in Table 4, the agreement between the results based on only 10 runs with those based on 20 runs is fairly good. Also note from table 4 that the coefficients of variation are similar in both cases. These are coefficients of variation for individual runs. The coefficient of variation for the average value will be smaller by a factor of $\sqrt{10}$ and $\sqrt{20}$ respectively.

Table 5. The relative distribution (%) taking a westerly route to the spawning grounds, an easterly route, and remaining in the north for six different simulation scenarios. Average values for the number of runs indicated. The value in parenthesis is the standard deviation estimated from the same runs.

Year	1994-95	2000-01	1994-95	2000-01	2000-01	2000-01
#particles	1096	1096	1096	1096	1096	283
#runs	10	10	20	20	10	10
Noiserange	80°	80°	80°	80°	20°	80°
Route						
West	0.4(0.4)	27.4(23.4)	0.3(0.3)	19.5(19.8)	43.7(21.4)	12.3(4.9)
East	94.1(2.6)	68.4(24.6)	94.2(3.8)	77.0(21.4)	55.4(21.9)	83.0(4.9)
North	5.5(2.4)	4.2(4.2)	5.5(3.7)	3.5(3.6)	0.9(1.0)	4.7(2.3)

In table 5 we show the fraction of particles taking the easterly and westerly route respectively to the spawning region. Again comparing the average values for 20 simulation runs with the results given in Dereksdóttir *et al*. (2003) we have that in the cold year 1994-95 94% take the easterly route instead of 93%, less than 1% take the westerly route instead of 2%, and 5% remain in the north in both cases. In the warm year 2000-01 77% take the easterly route instead of 80%, 19% take the westerly route

in both cases, and 4% stay in the north compared with 1%. Here it is also noteworthy that when the range of noise is reduced a smaller fraction (55%) takes the easterly route, whereas when the number of particles is reduced a larger fraction (83%) takes the easterly route (cf. Figure 11).

Discussion

While this simulation example demonstrates the feasibility of adopting the modelling approach presented above, it remains to carry out much more extensive experimentation in order to establish the sensitivity of the results to changes in parameter values. Following that it is obviously of interest to see how the parameters can be adjusted to obtain as good fit as possible with real acoustic measurements of capelin. From the point of view of computational efficiency it is further important to establish how many particles and how many simulation runs are needed in order to obtain stable results. The results presented above indicate that 1000 particles and 20 independent runs should prove sufficient.

As noted in the introduction, the approach of the triangularization of the simulation region introduced in this work has a number of advantages. In particular, it allows us to share data files and make effective comparisons with continuous migration models. As demonstrated above this facilitates comparisons of the results from the particle model with results obtained by the Kolmogorov continuous migration model described in Magnússon *et al*. (2004). In this respect it should be kept in mind that the output of the Kolmogorov model is the probability density of a fish being located at a given position at a given time subject to some initial probability distribution, whereas the output of particle model presented above is the actual position at a given time. Thus in order to obtain comparable results one has to make repeated runs of the stochastic particle model.

It is also of interest to compare the results of the particle model with the results of a continuous dynamic models like the one presented in Sigurdsson *et al*. (2002) where the output is the actual density of fish. It is e.g. of interest to establish how the particle model and the continuous model compare in terms of computational efficiency.

References

P. Babak, K. G. Magnússon, S. Th. Sigurdsson. 2004. Dynamics of group formation in collective motion of organisms, Mathematical Medicine and Biology, Volume 21, (4), 269-292

E. H. Dereksdóttir, K. G. Magnússon and S. Th. Sigurdsson. 2003. Simulations of spawning migrations of capelin in Icelandic waters based on temperature-current- and potential fields. Science Institute, University of Iceland, Report RH-16-2003

S. Hubbard, P. Babak, S. Th. Sigurdsson, K. G. Magnússon. 2004. A model of the formation of fish schools and migrations of fish. Ecological Modelling, 174, 359-374

K. G. Magnússon, S. Th. Sigurdsson, P. Babak, S. F. Gudmundsson, E. H. Dereksdóttir. 2004. A continuous density Kolmogorov type model for a migrating fish stock, Discrete and Continuous Dynamical Systems-Series B, Volume 4 (3), 695-704

K. G. Magnússon, S. Th. Sigurdsson, E. H. Dereksdóttir. (In press). A simulation model for capelin migrations in the North-Atlantic. Nonlinear Analysis: Real World Problems.

H.-S. Niwa. 1998. Migration dynamics of fish schools in heterothermal environments. J. theor. Biol., 193, 215-231.

A. Okubo and S.L. Levin. 2001. Diffusion and Ecological Problems: Modern Perspectives. Springer.

M.J.Reed and J.G.Balchen. 1982. A multidimensional continuum model of the fish dynamics and behaviour: Application to the Barents Sea capelin (*Mallotus villosus).* Modelling, Identification and Control, 3, 65-109.

S. Th. Sigurdsson, K. G. Magnússon, P. Babak, S. F. Gudmundsson, E. H. Dereksdóttir. 2002. Dynamic continuous model of fish migration, Science Institute, University of Iceland. Report RH-25-2002

J. Toner, J. and Y. Tu .1998. Flocks, herds and schools: A quantitative theory of flocking. Physical Review E, 58 (4), 4828-4858.

T. Vicsek, A. Czirok, E. Ben-Jacob, I. Cohen, O.Shochet. 1995. Novel type of phase transition in a system of self-driven particles. Phys. Rev. Lett. 75 (6), 1226-1229.

H. Vilhjálmsson.1994. The Icelandic capelin stock. Journal of the Marine Research Institute Reykjavik, Vol. XIII, No. 1. 281 pp.

H. Vilhjálmsson, H.N. Stefánsson, A.B. Lund, H. Sigurgeirsson and H. Björnsson. 1997. Capelin migrations. In BORMICON, A Boreal Migration and Consumption Model, G. Stefánsson and Ó.K. Pálsson (eds): Marine Research Report 58.

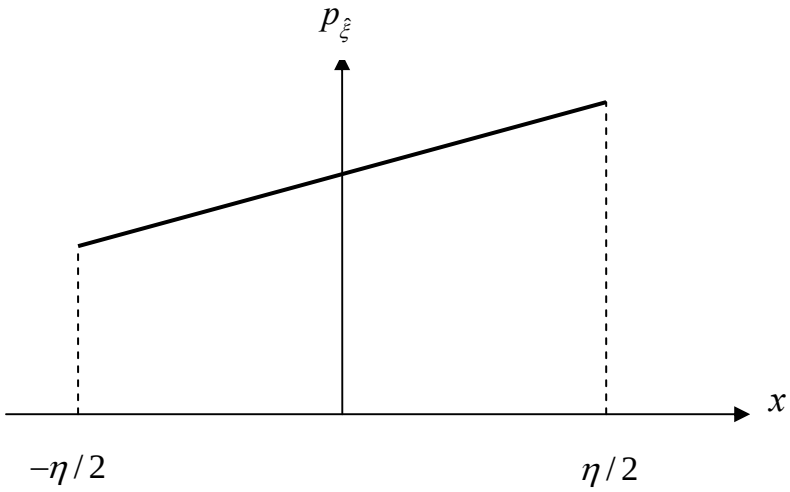

Figure 1. Probability density function of the random perturbation in direction angle.

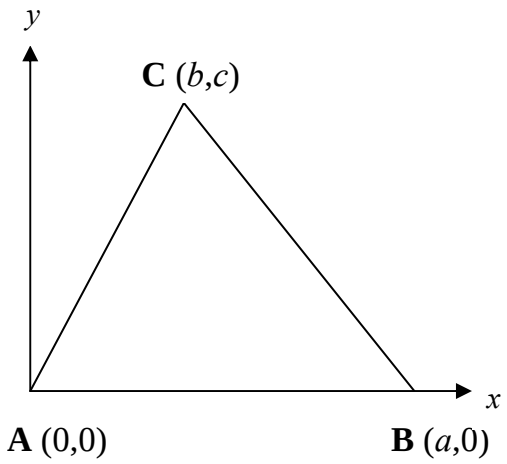

Figure 2. Local coordinates of triangular element.

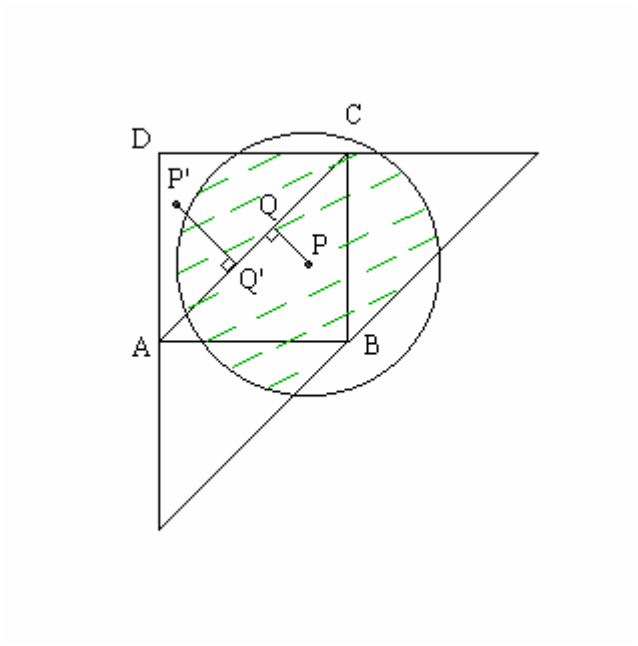

Figure 3. Circle of alignment around point *P.* Particles within the shaded area will affect the direction of a particle at *P.*

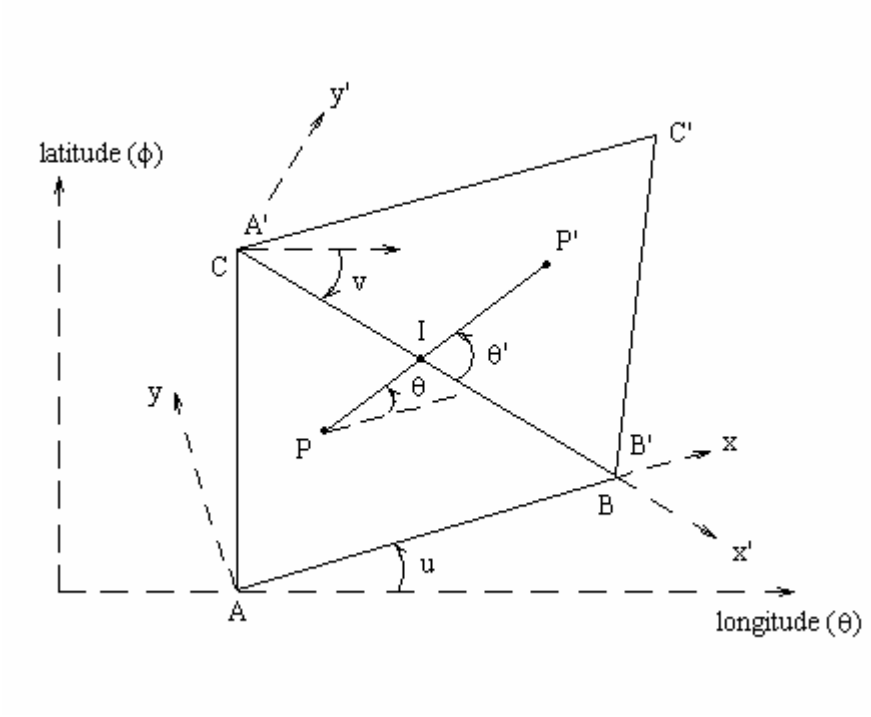

Figure 4. Relationship between local and global directions of motion as particle moves from one element into another.

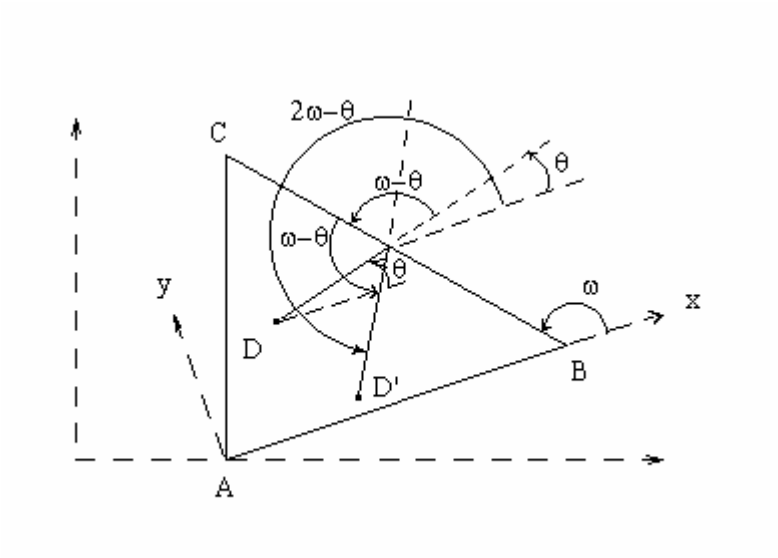

Figure 5. Relationship between local and global directions of motion as particle is reflected from land boundary.

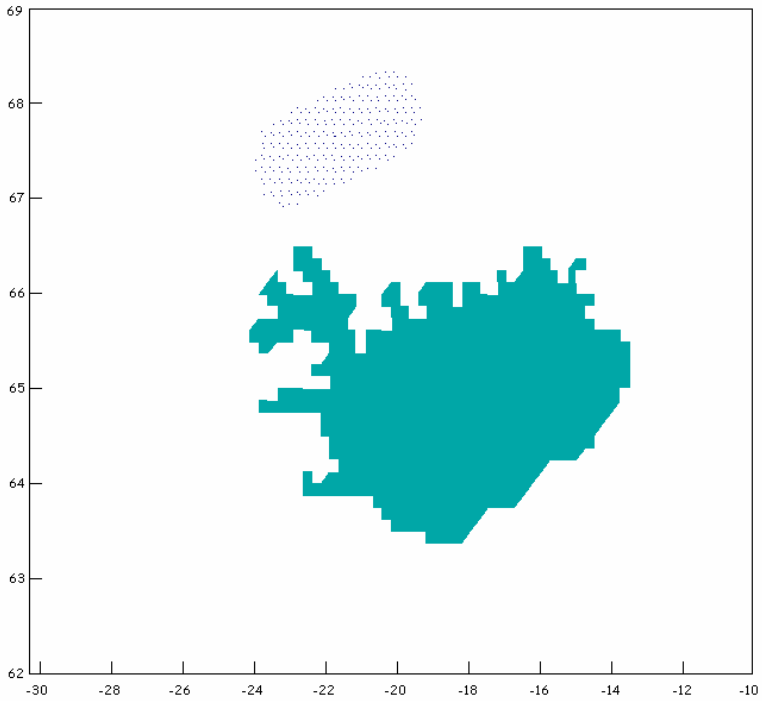

Figure 6. Area of simulation. The dots North-West of Iceland show the initial distribution of particles on October 1

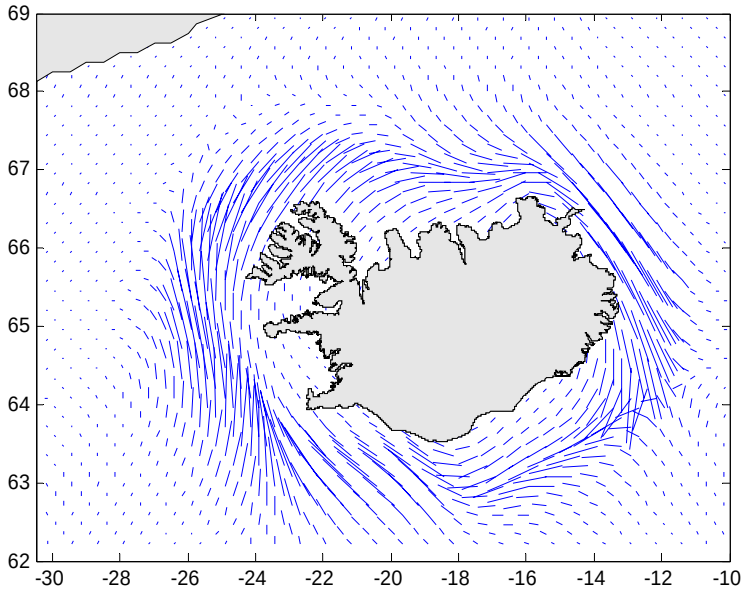

Figure 7. Hypothetical field of oceanic currents around Iceland. The speed of the current is given by the length of the arrows, i.e. darker colours indicate greater speed

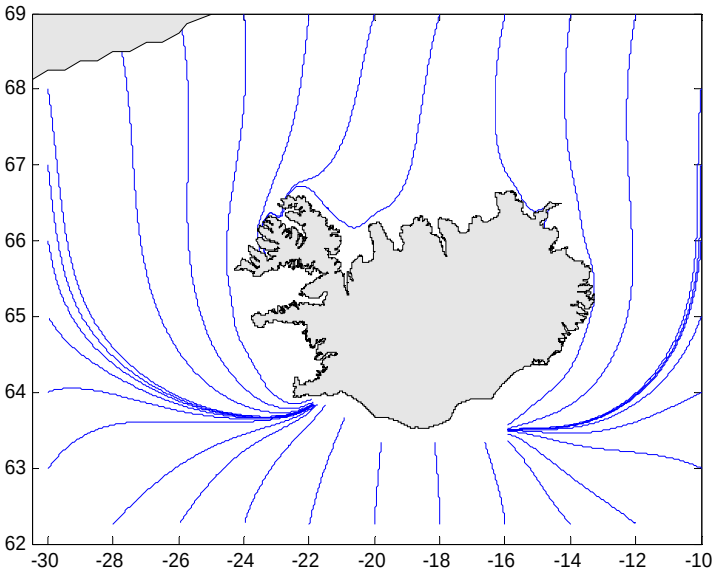

Figure 8. Iceland and the field lines for the attraction force generated by a spawning area on the south coast

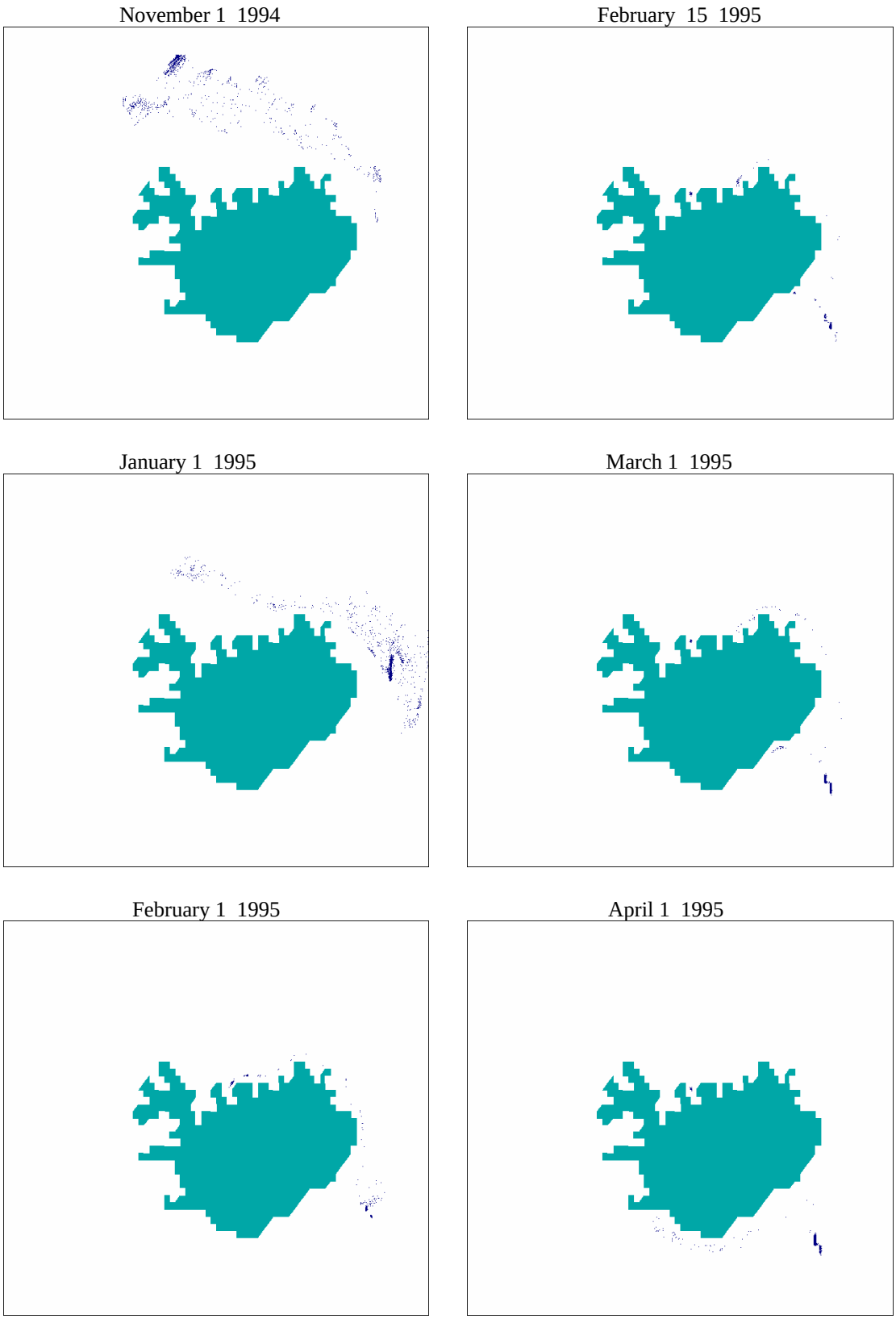

Figure 9. Snapshots of results from a simulation run with 1096 particles showing the migration of capelin from October 1 1994 until April 1 1995. The initial distribution on October 1 is shown in Figure 6.

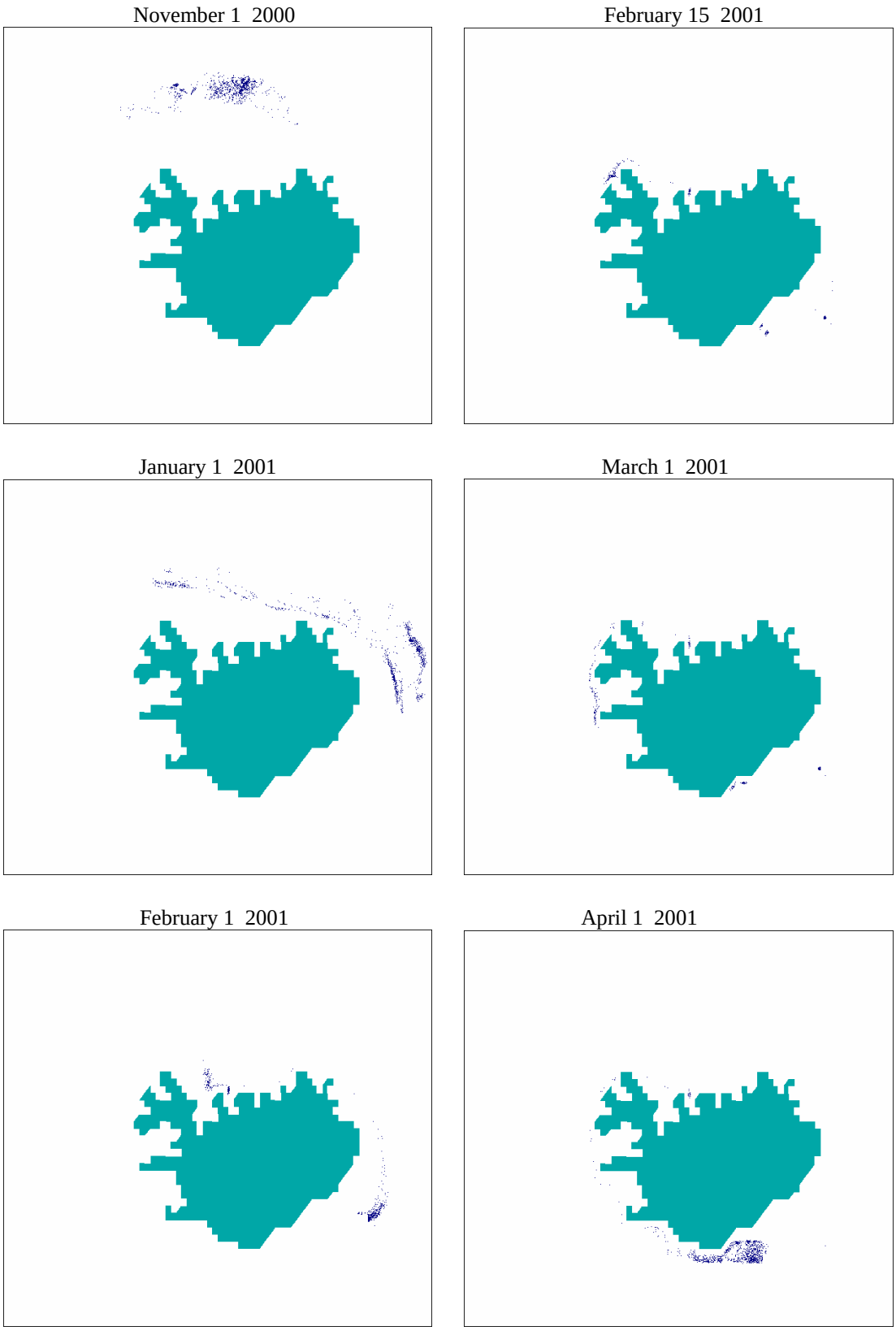

Figure 10. Snapshots of results from a simulation run with 1096 particles showing the migration of capelin from October 1 2000 until April 1 2001. The initial distribution on October 1 is shown in Figure 6.

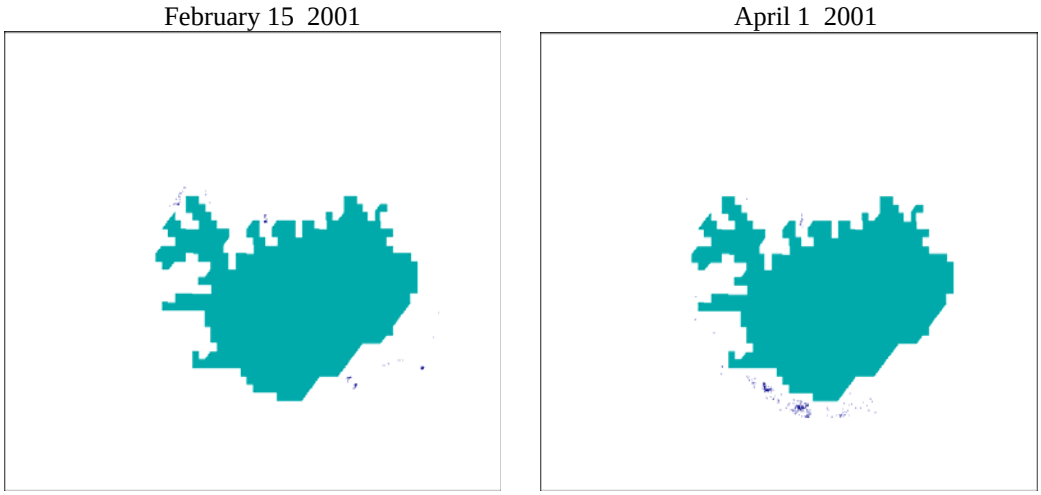

Figure 11. Two snapshots of results from a simulation run with 283 particles showing the migration of capelin from October 1 2000 until April 1 2001. The initial distribution on October 1 is shown in Figure 6.

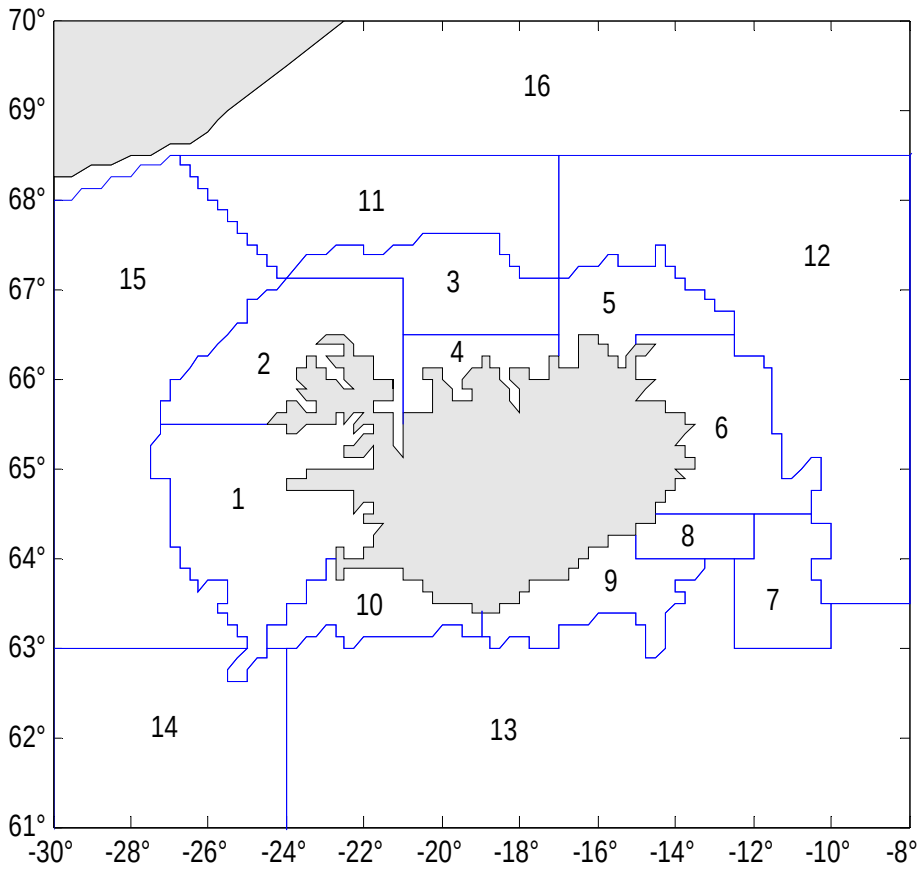

Figure 12. The sub-areas used in the transition matrix migration model for the waters around Iceland